JOURNAL OF AIRCRAFT
Vol. 32, No. 1, January–February 1995

Real-Time Estimation of Atmospheric Turbulence Severity from In-Situ Aircraft Measurements

Larry B. Cornman,* Corinne S. Morse,† and Gary Cunning‡
National Center for Atmospheric Research, Boulder, Colorado 80307

The quality of atmospheric turbulence detection and forecast information for the operational meteorology and aviation communities is directly linked to the quality of real-time measurements. Currently, the only direct data are subjective, qualitative, and intermittent pilot reports. This article describes techniques, suitable for real-time application on commercial transport aircraft, to generate quantitative and comprehensive turbulence measurements. These algorithms build on standard methods used in the analysis of aircraft response to turbulence, but are specifically designed to address the limitations of the available on-board data and computational resources.

Introduction

THROUGHOUT the latter half of this century, a great deal of research has been performed to better understand atmospheric turbulence. These wide ranging efforts dealt with turbulence phenomenology, in-situ and remote detection, numerical modeling, forecasting, and the response of aircraft flying through turbulent air.[1-3]

However, direct application of the resultant knowledge to operational meteorology and aviation has been somewhat limited. This is due, in large part, to an all too common problem: inadequate real-time measurements. Apart from the poor spatial and temporal resolution of the basic meteorological data that could be used to diagnose it, the only direct measurement of turbulence intensity currently available is from pilot reports (PIREPS).

The purpose of this article is to describe new, operationally useful techniques intended to provide adequate real-time, comprehensive, and direct atmospheric turbulence measurements. In brief, these methods would augment or replace the qualitative, intermittent, and subjective turbulence PIREPS with quantitative, "state-of-the-atmosphere" measurements.

These real-time and fully automated algorithms have been designed to run on commercial transport aircraft utilizing currently available data sources and computational capabilities. Computationally efficient methods have been developed to estimate eddy dissipation rates from aircraft vertical acceleration data. Computed turbulence measurements would then be appended to the winds and temperature reports currently broadcast via the Aircraft Communications Addressing and Reporting System (ACARS).

From this comprehensive and timely data base, both tactical and strategic turbulence products could be produced. For example, maps of detected turbulent airspace could provide accurate "heads-up" warnings to pilots and air traffic controllers. Furthermore, these quantitative, state-of-the-atmosphere measurements can be explicitly utilized by numerical weather models, in turn producing better forecasts of turbulence.

Received Nov. 14, 1993; presented as Paper 94-0268 at the AIAA 32nd Aerospace Sciences Meeting and Exhibit, Reno, NV, Jan. 10–13, 1994; revision received April 23, 1994; accepted for publication May 5, 1994.

*Associate Scientist. Member AIAA.
†Software Engineer.
‡Graduate Student Assistant.

Theoretical Background

Atmospheric turbulence is inherently a four-dimensional phenomenon. Unfortunately, with the data available on-board commercial aircraft, the complete resolution of the turbulent airflow characteristics is impossible. Therefore, we seek a set of simplifying assumptions that will allow for a more tractable analysis. In this section an outline of this simplification process is presented. Furthermore, an important connection between the mathematical descriptions often employed by atmospheric scientists and aerodynamicists is established.

Energy Spectrum

One way to describe the properties of the turbulent flow is through the velocity correlation tensor[2,4]

$$R_{ij}(\boldsymbol{x}, \boldsymbol{\xi}, t) = \langle u_i(\boldsymbol{x}, t), u_j(\boldsymbol{x} + \boldsymbol{\xi}, t) \rangle \tag{1}$$

If we assume that the flowfield is spatially homogenous, and temporally stationary, the (spatial) Fourier transform of the correlation tensor yields the energy-spectrum tensor:

$$\Phi_{ij}(\boldsymbol{k}) = \frac{1}{8\pi^3} \int_{-\infty}^{\infty} R_{ij}(\boldsymbol{\xi}) e^{\,i(\boldsymbol{k}\cdot\boldsymbol{\xi})}\, \mathrm{d}\boldsymbol{\xi} \tag{2}$$

The assumption of spatial homogeneity allows for the use of the ergodic hypothesis, i.e., the ensemble average $\langle\ \rangle$ can be replaced by a spatial average. Furthermore, this assumption means that the correlation tensor is not a function of location $\boldsymbol{x}$, merely the spatial lag, $\boldsymbol{\xi}$. The assumption of temporal stationarity implies that the statistical properties of the velocity field are not changing with time.

Next, the assumption of spatial isotropy is invoked. This implies that the energy tensor is invariant under rotation and reflection of the coordinate axes. Hence, it is convenient to express Eq. (2) in spherical polar coordinates and integrate over the angular dimensions. Denoting the length of the wave number vector as $k = |\boldsymbol{k}|$, the three-dimensional energy spectrum (scalar) function is then defined as

$$E(k) = 2\pi k^3 \Phi_{ii}(k) \tag{3}$$

This expression gives the amount of kinetic energy in a spherical shell of wave number space, such that

$$\int_0^{\infty} E(k)\, \mathrm{d}k = \frac{3}{2}\sigma_i^2 \tag{4}$$

where σ_i^2 refers to the mean square value of any of the orthogonal ($i = u$, v, or w) velocity components.

The isotropy assumption can also be used to establish the important connection between the three-dimensional energy spectrum and the one-dimensional spectrum. This relationship for the transverse ("2") velocity component along the longitudinal ("1") direction is given by

$$\phi_2(k_1) = \frac{1}{2}\int_{k_1}^{\infty} \frac{E(k)}{k}\left(1 + \frac{k_1^2}{k^2}\right) dk \tag{5}$$

For the analysis below, the case of interest will be for the transverse (vertical) velocity along the longitudinal (flight path) direction.

In order to apply Eq. (5), a specific form of the energy spectrum must be assumed. In the study of atmospheric turbulence, the atmospheric scientist generally refers to the Kolmogorov form, while the aerodynamicist typically uses the von Kármán form.

Kolmogorov Energy Spectrum

Under the assumptions of isotropy and large Reynolds number, Kolmogorov[5] hypothesized that there exists a range of wave numbers wherein the inertial transfer of energy is dominant. That is, within this so-called "inertial subrange," turbulent energy is neither produced nor dissipated, but is transferred inertially from larger to smaller eddies. By dimensional analysis, Kolmogorov was able to show that within the inertial subrange the energy spectrum can only depend on one parameter, ε, the eddy dissipation rate and that the functional dependence must be

$$E(k) = A\varepsilon^{2/3}k^{-5/3} \tag{6}$$

where A is a numerical constant. The dissipation rate describes how fast the turbulent energy is converted into heat by viscous effects at wave numbers above the inertial subrange. Within the context of forecasting atmospheric turbulence from numerical weather models, the eddy dissipation rate is a key parameter.

Von Kármán Energy Spectrum

Unfortunately, there does not yet exist a comprehensive theory that yields an experimentally verified functional form of the energy spectrum across all wave numbers. Theoretical and experimental evidence does indicate the existence of the Kolmogorov form indicated above, as well as a k^4 dependence at very small wave numbers. Based on this information von Kármán[6] introduced an interpolation formula (valid for very large Reynolds numbers) between the k^4 and $k^{-5/3}$ regimes. This energy spectrum is

$$E(k) = \frac{55}{9}\frac{\Gamma(\frac{5}{6})}{\Gamma(\frac{1}{3})\sqrt{\pi}}\frac{\sigma_i^2}{k_0}\frac{(k/k_0)^4}{[1 + (k/k_0)^2]^{17/6}} \tag{7}$$

where σ_i^2 is as described in Eq. (4) above, $\Gamma(\ )$ is the gamma function, and k_0 will be discussed below. In the limit of large k/k_0, Eq. (7) becomes

$$E(k) \to \frac{55}{9}\frac{\Gamma(\frac{5}{6})}{\Gamma(\frac{1}{3})\sqrt{\pi}}\frac{\sigma_i^2}{k_0}(k/k_0)^{-5/3} \tag{8}$$

The one-dimensional vertical gust velocity spectrum that will be used herein, is obtained by inserting Eq. (7) into Eq. (5), and integrating, to yield

$$\phi_{w_g}(k_1) = \frac{\Gamma(\frac{5}{6})}{\sqrt{\pi}\Gamma(\frac{1}{3})}\frac{\sigma_w^2}{k_0}\frac{1 + \frac{8}{3}(k_1/k_0)^2}{[1 + (k_1/k_0)^2]^{11/6}} \tag{9}$$

This form of the velocity spectrum is what would be computed from vertical velocities measured by a gust probe mounted on an aircraft flying through the turbulent airspace.

Connection Between the Spectral Forms

Inspection of Eqs. (6) and (8) indicate that the former is a function of the single parameter ε, whereas the latter is a function of the two parameters, k_0 and σ_i^2. The relationship among these three parameters is now established. Equating Eqs. (6) and (8), and solving for $\varepsilon^{2/3}$, gives

$$\varepsilon^{2/3} = \left(\frac{1}{A}\right)\frac{55}{9}\frac{\Gamma(\frac{5}{6})}{\sqrt{\pi}\Gamma(\frac{1}{3})}\sigma_w^2 k_0^{2/3} \tag{10}$$

Next, the relationship between the wave number k_0, and the integral length scale is derived. The convention in the aerodynamic literature is to use the longitudinal length scale L_u, whose value is given by

$$L_u = \frac{\pi}{\sigma_w^2}\phi_{w_g}(0) = \frac{\Gamma(\frac{5}{6})}{\Gamma(\frac{1}{3})}\frac{\sqrt{\pi}}{k_0} \tag{11}$$

Inserting the value of k_0 obtained from Eq. (11) into Eq. (10) yields the desired relation that connects the Kolmogorov and von Kármán energy spectrum forms

$$\varepsilon^{2/3} = \frac{55}{9}\frac{1}{A(\pi)^{1/6}}\left[\frac{\Gamma(\frac{5}{6})}{\Gamma(\frac{1}{3})}\right]^{5/3}\frac{\sigma_w^2}{L_u^{2/3}} \tag{12}$$

where the units of ε are m^2/s^3. Finally, the form of the one-dimensional velocity spectrum (in terms of the eddy dissipation rate), valid in the inertial subrange is derived. Using Eqs. (10) and (11), Eq. (9) can be rewritten as

$$\phi_{w_g}(k_1) = \left[\frac{\Gamma(\frac{5}{6})\sqrt{\pi}}{\Gamma(\frac{1}{3})L_u}\right]^{-5/3}\frac{9A\varepsilon^{2/3}}{55}\frac{1 + \frac{8}{3}(k_1/k_0)^2}{[1 + (k_1/k_0)^2]^{11/6}} \tag{13}$$

The large wave number approximation is given by

$$\phi_{w_g}(k_1) \to \left(\frac{24}{55}A\right)\left[\frac{\Gamma(\frac{5}{6})\sqrt{\pi}}{\Gamma(\frac{1}{3})L_u}\right]^{-5/3}\varepsilon^{2/3}\left(\frac{k_1}{k_0}\right)^{-5/3} \tag{14}$$

Eliminating k_0, by Eq. (11) gives the desired result [denoting the large wave number approximation by $\hat{\phi}_{w_g}(k_1)$]

$$\hat{\phi}_{w_g}(k_1) = \frac{24}{55}A\varepsilon^{2/3}k_1^{-5/3} \approx 0.7\varepsilon^{2/3}k_1^{-5/3} \tag{15}$$

where in the last step the value of $A = 1.6$ was used.[7] It should be noted that this equation can also be obtained by inserting Eq. (6) into Eq. (5), limiting the range of k_1 to those in the inertial subrange.

Methodology

The techniques developed below are based on straightforward modifications to power-spectral, linear-system frequency response analysis of aircraft response to turbulence. Given the power spectral density (psd) of the input vertical gust velocities $\phi_{w_g}(\omega)$, and the modulus square of the frequency response function relating (c.g.) vertical acceleration to the gust input, we can compute the psd of the acceleration response:

$$\phi_{\ddot{z}}(\omega) = \left|\frac{\ddot{z}(i\omega)}{w_g(i\omega)}\right|^2\phi_{w_g}(\omega) \tag{16}$$

The formulation is made in the temporal-frequency domain since the measurements are made by aircraft flying through the turbulent airspace at speed V, where $\omega = k_1 V$. Taylor's "frozen-field" hypothesis[8] is easily satisfied for the combination of aircraft airspeed and turbulence length scales of

interest, hence we can analyze the spatial characteristics of the turbulence via the temporal aircraft measurements.

We will be interested in a limited range of frequencies, and so integrating Eq. (16) between two frequencies, ω_1 and ω_2, gives the response power contained in that frequency range $\hat{\sigma}_{\dot{z}}^2$, given by

$$\hat{\sigma}_{\dot{z}}^2 \equiv \int_{\omega_1}^{\omega_2} \phi_{\dot{z}}(\omega)\, d\omega = \int_{\omega_1}^{\omega_2} \left| \frac{\ddot{z}(i\omega)}{w_g(i\omega)} \right|^2 \phi_{w_g}(\omega)\, d\omega \quad (17)$$

The proper choice of the cutoff frequencies is critical, and as will be discussed below, they are selected to be compatible with the simplifying assumptions made herein. Briefly, these simplifications relate to the use of a rigid-body, two degree-of-freedom aircraft response model, the resolution of available real-time data, and an assumed form for the gust psd. In practice, a bandpass filter is applied to the acceleration data, and hence, we should write Eq. (17) as

$$\hat{\sigma}_{\dot{z}}^2 \approx \int_0^{\infty} |H_{bp}(\omega_1, \omega_2, \omega)|^2 \left| \frac{\ddot{z}(i\omega)}{w_g(i\omega)} \right|^2 \phi_{w_g}(\omega)\, d\omega \quad (18)$$

where ω_1 and ω_2 correspond to the filter's half-power points.

For the typical flight conditions of commercial transport aircraft, the frequency band within which the majority of the rigid body aircraft vertical acceleration response occurs corresponds to the inertial subrange of atmospheric turbulence. We therefore assume the following approximate form for the gust psd [cf. Eq. (15)]:

$$\hat{\phi}_{w_g}(\omega) \equiv 0.7V^{2/3}\varepsilon^{2/3}\omega^{-5/3} \quad (19)$$

Inserting Eq. (19) into Eq. (18) yields

$$\hat{\sigma}_{\dot{z}}^2 = 0.7V^{2/3}\varepsilon^{2/3} \int_0^{\infty} |H_{bp}(\omega_1, \omega_2, \omega)|^2 \left| \frac{\ddot{z}(i\omega)}{w_g(i\omega)} \right|^2 \omega^{-5/3}\, d\omega \quad (20)$$

Hence, if the aircraft response function is known and the power in the filtered acceleration signal is measured, an estimate of the dissipation rate can be made.

In practice, the cutoff frequencies, ω_1 and ω_2 are selected as follows. The lower cutoff must be greater than the (unmodeled) phugoid response frequencies, low-frequency pilot-induced maneuver effects, and above an assumed combination of minimum aircraft airspeed and turbulence integral length scale L_u. This third condition relates to a frequency regime where the $\omega^{-5/3}$ assumption is valid. The high-end cutoff frequency is made to lie below the elastic response modes of the given aircraft and the Nyquist frequency of the acceleration data. Typically, these values are on the order of $\omega_1 = 0.1$ Hz and $\omega_2 = 1.0$ Hz.

In the preceding development, the assumption of spatial homogeneity has been made. Unfortunately, atmospheric turbulence is not truly homogenous, and hence, Eq. (18) should more properly be written as

$$\hat{\sigma}_{\dot{z}}^2(t) = \int_0^{\infty} |H_{bp}(\omega_1, \omega_2, \omega)|^2 \left| \frac{\ddot{z}(i\omega)}{w_g(i\omega)} \right|^2 (t)\phi_{w_g}(\omega, t)\, d\omega \quad (21)$$

However, under conditions wherein the spatial dimension (along the flight path) of the inhomogeneity is large relative to the integral length scale of the underlying turbulence,[9] we can write

$$\hat{\phi}_{w_g}(\omega, t) \equiv 0.7V^{2/3}(t)\varepsilon^{2/3}(t)\omega^{-5/3} \quad (22)$$

That is, the spectral "functional form" does not vary with time, but the relative amplitude does (local homogeneity). Indicating the time-dependence of the terms in Eq. (20) and solving for the eddy dissipation rate (to the two-thirds power), yields

$$\varepsilon^{2/3}(t) = \frac{\hat{\sigma}_{\dot{z}}^2(t)}{0.7V^{2/3}(t)I(\omega_1, \omega_2, t)} \quad (23)$$

where $I(\omega_1, \omega_2, t)$ denotes the integral in Eq. (20), and the time-dependency relates to the variation of the aircraft response function with flight condition, i.e., Mach number, altitude, and aircraft mass.

Within the aerodynamic community, the use of the von Kármán spectrum has been a matter of controversy and confusion. This problem relates to the independent measurement of the integral length scale and the mean-square value from turbulence data, appropriate choices for these parameters in aircraft design studies and certification, and even more fundamentally, whether the von Kármán spectrum is a proper description of the atmosphere. However, as the author of Ref. 2 has pointed out, a more suitable intensity metric is the combined parameter $\sigma_w^2/L_w^{2/3}$, which we have shown to be directly proportional to the eddy dissipation rate.

The use of the eddy dissipation rate is well-established by atmospheric scientists as an objective measure of atmospheric turbulence intensity,[3,10] and various methods have been used to calculate it from research aircraft data.[11,12] Our real-time formulation for estimating this parameter from commercial aircraft data is unique in that it utilizes a two degree-of-freedom aircraft model—with autopilot—and that the inherent limitations of the data, the aircraft response, and turbulence models are explicitly accounted for.

In the next sections, the computation of the right side of Eq. (23) is discussed.

Aircraft Response Function

In this section the c.g., vertical acceleration response function is developed. The choice of a (short-period) two degree-of-freedom model (pitch and plunge)—while inherently more complicated than the usual plunge-only model—is essential to the accurate calculation of aircraft response to continuous turbulence.[13] Furthermore, it can be shown that the inclusion of autopilot effects is of similar importance.[14] The requirements that this model must meet, besides computational ease and relative accuracy are, applicability to any aircraft, explicit inclusion of varying flight conditions, formulation without manufacturer-supplied data (although it can be incorporated whenever available), and a direct relation to available onboard measurements.

Implicit in the model is that 1) The aircraft is a rigid body, with two degrees of freedom (DOF)—vertical motion z and pitch θ; 2) lift forces for the wing and horizontal tail surfaces act at their $\frac{1}{4}$-chord points, and are given by the downwash velocities at their $\frac{3}{4}$-chord points, respectively; 3) first-order corrections are made for Mach number, aspect ratio, sweepback, and (if available) flexibility effects via effective lift curve slope values; 4) first-order corrections are made for unsteady aerodynamic gust penetration (Küssner) effects; and 5) quasi-steady wing downwash effects on the tail are included.

The equations of motion are then given by[15]

$$m\ddot{z}(t) = L_w(t) + L_t(t) \quad (24)$$

$$mr^2\ddot{\theta}(t) = eL_w(t) - e_tL_t(t) \quad (25)$$

where m is the total aircraft mass, r is the pitch radius of gyration, e and e_t are the distances from the c.g. to the one-quarter-chord of the wing and tail, respectively. The lift forces

on the wing L_w and the tail L_t are given by (suppressing the time dependency)

$$L_w(t) = \frac{1}{2} a\rho SV\{V\theta - \dot{z} - [e - (c/2)]\dot{\theta} + w_g\} \quad (26)$$

$$L_t(t) = \tfrac{1}{2}a_t\rho S_t V\big(VF_\delta\delta_e + (V\dot{\theta} - \dot{z} + w_g)(1 - \varepsilon_\alpha) + \{e_t + (c_t/2) + \varepsilon_\alpha[e - (c/2)]\}\dot{\theta}\big) \quad (27)$$

where a is the lift curve slope, S is the reference surface area, c is the mean aerodynamic chord, ρ is the air density, $\varepsilon_\alpha = d\varepsilon/d\alpha$ is the downwash factor (not to be confused with ε, the eddy dissipation rate), δ_e is the elevator angle, and F_δ is the elevator effectiveness.

Inserting Eqs. (26) and (27) into Eqs. (24) and (25) results in a coupled set of second-order linear differential equations, subjected to two forcing functions: w_g and δ_e. Taking Laplace transforms, (assuming zero initial conditions) yields a system of linear algebraic equations for the Laplace transform of the vertical displacement $z(s)$ and pitch angle $\theta(s)$:

$$\begin{bmatrix} a_{11}(s) & a_{12}(s) \\ a_{21}(s) & a_{22}(s) \end{bmatrix} \begin{bmatrix} z(s) \\ \theta(s) \end{bmatrix} = \begin{bmatrix} b_{11}(s) & b_{12}(s) \\ b_{21}(s) & b_{22}(s) \end{bmatrix} \begin{bmatrix} \delta_e(s) \\ w_g(s) \end{bmatrix} \quad (28)$$

where the a_{ij} and b_{ij} are polynomials in s, whose coefficients are functions the parameters of Eqs. (24–27).

Solving for $z(s)$ and $\theta(s)$

$$\begin{bmatrix} z(s) \\ \theta(s) \end{bmatrix} = A^{-1}B \begin{bmatrix} \delta_e(s) \\ w_g(s) \end{bmatrix} = \frac{C}{\Delta_A(s)} \begin{bmatrix} \delta_e(s) \\ w_g(s) \end{bmatrix} \quad (29)$$

where $\Delta_A(s) = \det A$, and $C = (\text{adj } A)B$.

We next assume that the elevator angle is controlled by an autopilot, and that within the frequency range of interest it can be modeled via an appropriate pitch feedback transfer function: $G_\theta(s)$. Hence, we can write

$$\delta_e(s) \approx -G_\theta(s)\theta(s) \quad (30)$$

Plugging this into Eq. (29) yields

$$\frac{\ddot{z}(s)}{w_g(s)} = \frac{s^2 z(s)}{w_g(s)} = s^2 \left[\frac{c_{12}(s) - G_\theta(s)\Delta_B(s)}{\Delta_A(s) + G_\theta(s)c_{21}(s)}\right] \beta(s) \quad (31)$$

where c_{21}, c_{12}, and $\Delta_B(s) = \det B$ are all polynomials in s; and $\beta(s)$ is a function taking into account the unsteady aerodynamic effects.[15] Replacing s by $i\omega$, and taking the modulus-squared of Eq. (31) gives the desired result.

Evaluation of the Integral

Even with a very simple autopilot model, the modulus square of the aircraft response function will be a ratio of fairly high-order polynomials. After multiplying this function by the spectrum and bandpass filter functions, the complexity of the resultant integrand [c.f., Eq. (20)] precludes an exact closed-form evaluation. Numerical evaluation is possible, though inefficient, and because the integrand is a function of differing flight conditions, we seek a closed-form approximation.

The first step entails the replacement of the $\omega^{-5/3}$ function with an approximate ω^{-2} function:

$$\hat{\phi}_{w_g}(\omega)|\beta(i\omega)|^2 = \chi\varepsilon^{2/3}\omega^{-2} \quad (32)$$

by defining a term χ such that

$$0.7V^{2/3}|\beta(i\omega_s)|^2\omega_s^{-5/3} = \chi\omega_s^{-2} \quad (33)$$

where ω_s is the aircraft's (without autopilot) short-period undamped natural frequency. Furthermore, we assume that the bandpass filter function is an idealized unit amplitude rectangle in the frequency domain. With these simplifications, we can write Eq. (20) as

$$\frac{\hat{\sigma}_{\ddot{z}}^2}{\varepsilon^{2/3}} \approx \chi \int_{\omega_1}^{\omega_2} \frac{N_m(\omega)}{D_m(\omega)D_m(-\omega)}\, d\omega \quad (34)$$

where $N_m(\omega)$ and $D_m(\omega)$ are of the form

$$N_m(\omega) = b_0\omega^{2m-2} + b_1\omega^{2m-4} + \cdots + b_{m-1}$$
$$D_m(\omega) = a_0\omega^m + a_1\omega^{m-1} + \cdots + a_m$$

The order of the polynomials is determined by the explicit form of the autopilot transfer function. For example, if we chose an autopilot model containing a (first-order lag) actuator, with pitch and pitch rate feedback

$$G_\theta(s) = [K/(s + K_a)](K_\theta + K_{\dot{\theta}}s) \quad (35)$$

where K is an overall gain, K_a is the actuator inverse time-constant, and K_θ and $K_{\dot{\theta}}$ are the pitch and pitch rate gains, respectively. With this autopilot model, Eq. (34) is of the form

$$\frac{\hat{\sigma}_{\ddot{z}}^2}{\varepsilon^{2/3}} \approx \chi \int_{\omega_1}^{\omega_2} \frac{b_0\omega^6 + b_1\omega^4 + b_2\omega^2 + b_3}{|a_0\omega^4 + a_1\omega^3 + a_2\omega^2 + a_3\omega + a_4|^2}\, d\omega \quad (36)$$

This is not integrable in closed form, however, we can write

$$\int_{\omega_1}^{\omega_2} \frac{N_m(\omega)\, d\omega}{D_m(\omega)D_m(-\omega)} = \int_0^\infty - \int_0^{\omega_1} - \int_{\omega_2}^\infty \frac{N_m(\omega)}{D_m(\omega)D_m(-\omega)}\, d\omega \quad (37)$$

Consider each of the integrals on the right side. When all of the roots of $D_m(\omega)$ are in the upper half-plane (a condition that will be assured here, since our aircraft-autopilot model must be a stable system), evaluation of the first integral can be made via a contour integral.[16] This method is fortuitous in that the computation of the roots is not required. The second two integrals on the right side can be evaluated by making low- and high-frequency approximations to the integrand, respectively. The final form of the integral approximation, is a complicated, though easily computed function of a given aircraft/flight condition parameter set, as required.

Evaluation of $\hat{\sigma}_{\ddot{z}}^2$

From Eq. (17), it is seen that the aircraft response mean-square value $\hat{\sigma}_{\ddot{z}}^2$ is determined via the integral of the response psd between ω_1 and ω_2. Continuing with our attempts at computational efficiency, we seek an alternative to calculating and then integrating the psd in real-time.

This procedure[16] involves writing the power spectrum in its periodogram form, applying Parseval's theorem (assuming local-stationarity), and then using the convolution theorem to yield the approximation:

$$\hat{\sigma}_{\ddot{z}}^2(t) \approx \frac{1}{2T}\int_{t-T}^{t+T} \left[\int_0^{\tau_1} h_{bp}(\tau_2)\ddot{z}(\tau_1 - \tau_2)\, d\tau_2\right]^2 d\tau_1 \quad (38)$$

where $h_{bp}(\tau)$ is the inverse Fourier transform of $H_{bp}(\omega_1, \omega_2, \omega)$. This equation merely states that the frequency-limited response mean-square value is obtained by computing a running mean-square value of the bandpass filtered acceleration signal. The use of this time-domain formulation is also more appropriate to situations in which the turbulence intensity is fairly inhomogeneous, i.e., the oft-encountered "turbulent-patches." In practice Eq. (38) is discretized—the integrals replaced with summations. Furthermore, nonzero mean values are removed in the computation of the outer integral (summation). The averaging interval $2T$ is selected to satisfy

the local-stationarity assumption and provide enough data values for statistical stability. The time constant τ_1, is chosen such that $h_{bp}(\tau) \to 0$ for $\tau > \tau_1$.

Results and Discussion

In this section, a brief analysis of the methods described above is made.

Aircraft Response Model

Figure 1 compares the modulus of our computed response model for a typical short-haul transport aircraft with curves supplied by the manufacturer (for two extremal locations of the center of gravity). For simplicity, these models do not contain autopilot or unsteady aerodynamic effects. Clearly, the use of a two degree-of-freedom model is required.

It is also important to note the effect of moving the location of c.g.—something that will vary with flight condition and mass distribution. The c.g. location is an explicit quantity in our model, and since its real-time location can only be estimated, it is probably the largest source of error herein. Fortunately, in our method, the pertinent quantity is proportional to the area under these curves [cf., Eq. (17)], a value that turns out to be fairly constant with varying c.g. location.

Figure 2 illustrates the relative accuracy of the aircraft model for the NCAR King Air. Comparisons are made between modeled and measured acceleration spectra, [i.e., the integrand of Eq. (20), without bandpass filter, and normalized to unit ε]. This example is perhaps misleading in its accuracy, as the autopilot parameters for this aircraft were chosen (to achieve a target damping ratio) for this flight condition. The accuracy was not quite as good for other flight conditions and for the other, larger aircraft (note: each aircraft has its own set of gains).

The effect of the attitude-hold autopilot model is as expected: the short period damping and undamped natural frequency are increased.[17] Furthermore, it can be seen that the two-dimensional aircraft model with autopilot lies between the one-dimensional and two-dimensional (without autopilot) models. It should be noted that the autopilot that was actually engaged during this flight leg was an altitude-hold one. It can be assumed that some form of pitch feedback is also employed in this mode, so that the attitude-hold model is suitable in the frequency range of interest.

For this figure and subsequent ones, linear frequencies are used $f = \omega/2\pi$, and the frequencies of interest have a far greater range than the amplitudes. Hence, the vertical axes are multiplied by frequency so that a linear-log plot maintains the same area proportionality between two frequencies as in a linear-linear one, i.e.,

$$\int_a^b \Psi(f)\, df = \int_a^b f\Psi(f)\, d(\log f) \tag{39}$$

Integral Approximation

In this section, the accuracy and sensitivity of the approximation of the integral, Eq. (20), is examined. Various assumptions are made in the approximation process, including the use of the high-frequency forms ($\omega^{-5/3}$, and ω^{-2}) of the gust spectrum, ignoring the specific form of the bandpass filter, and the use of the low- and high-frequency approximations of the integrand.

Figure 3 illustrates the normal acceleration response of the four aircraft analyzed in this study. The full von Kármán spectrum, Eq. (13), was used with a unit value of $\varepsilon^{2/3}$, and an integral length scale of 762 m. The cutoff frequencies for the bandpass filter were selected as $f_1 = \omega_1/2\pi = 0.1$ Hz for all the aircraft, and $f_2 = \omega_2/2\pi = 0.8$–$2.0$ Hz from largest to smallest aircraft. These upper values were selected to lie below first wing bending mode frequencies. The amount of power outside the cutoff frequencies, which is larger for other flight conditions, illustrates the need to remove their contribution to the overall integral [cf., Eq. (37)].

Next, we examine the effect of making the $\omega^{-5/3}$ approximation in the von Kármán spectral form. Figure 4 illustrates this situation using the "cruise" flight condition for the large commercial transport aircraft. As expected, the difference occurs only at lower frequencies, and for this case would not greatly effect the overall integral. This effect can become large for certain combinations of flight condition and integral length scale. However, the cases with the largest fractional error occur in relatively extreme conditions, i.e., small integral length scales for the corresponding altitudes.

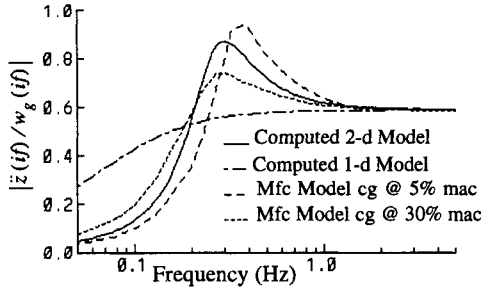

Fig. 1 Comparison of the modulus of the computed aircraft response function with manufacturer supplied values (small commercial transport 0.75*M* at 35,000 ft).

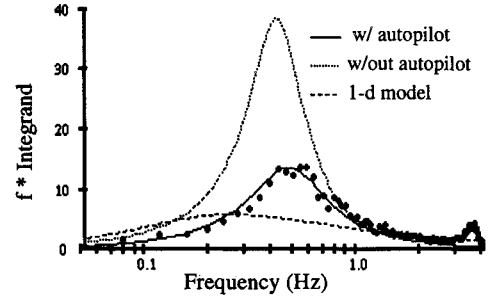

Fig. 2 Comparison of aircraft model with flight data (Super King Air B-200T in cruise).

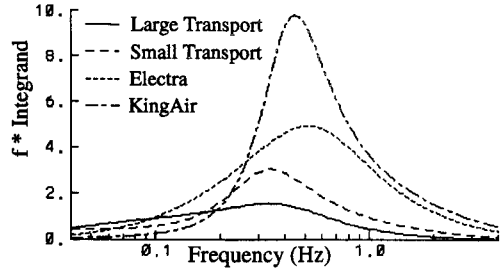

Fig. 3 Normal acceleration response for difference aircraft (comparison of aircraft response in cruise with autopilot).

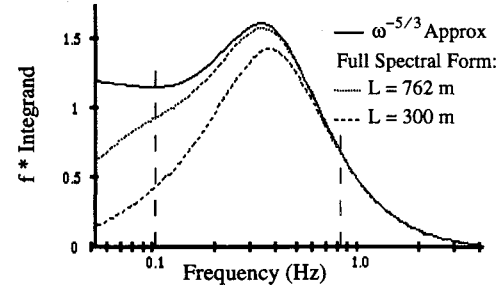

Fig. 4 Effect of the full von Kármán spectrum vs $\omega^{-5/3}$ approximation. Vertical lines indicate cutoff frequencies (large commercial transport in cruise).

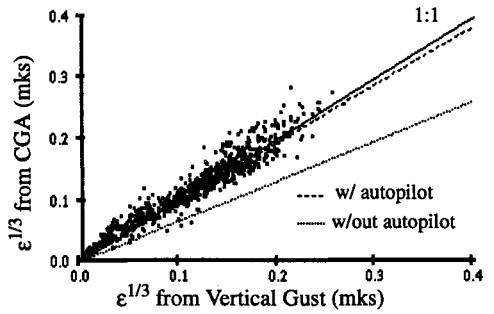

Fig. 5 One-minute median eddy dissipation rate values from vertical gust velocities vs derived values. Data from research aircraft. Correlation coefficient is 0.97.

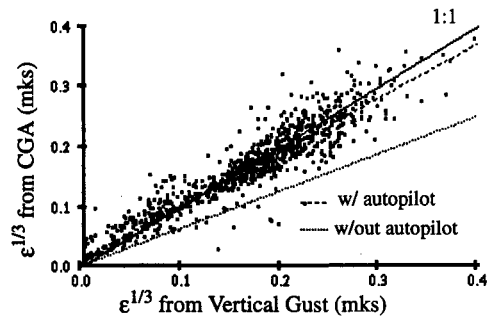

Fig. 6 One-minute 90th percentile eddy dissipation rate values from vertical gust velocities vs derived values. Data from research aircraft. Correlation coefficient is 0.93.

Dissipation Rate Calculations

Finally, all of the above theoretical concepts are applied to actual flight data. Three sets of data are analyzed: "research quality" data from the NCAR King Air and NCAR Electra, and "lower-quality" data from several large transport aircraft. The King Air and Electra flights, totaling 750 and 193 min, respectively, were through light to moderate turbulence. These flights reflect a large range of flight conditions, however for simplicity, the autopilot parameters for a given aircraft were not varied. The transport aircraft data were from five short, severe encounters,[18] totalling 29 min.

It is important to discuss the procedure used in obtaining the eddy dissipation rates portrayed in the subsequent figures. First, the raw vertical acceleration data (20 Hz for the King Air and Electra flights, and 4 Hz for the transport cases), were passed through the bandpass filter and the mean-square values were computed [c.f., Eq. (38), with $2T = 10$ s]. Note that these running mean-square values are obtained at every data update, i.e., every 0.05 s for the research data, and every 0.25 s for the transport data. Next, these values are used with Eq. (23) to compute the eddy dissipation rate values, again at every data update. It should be noted that the aircraft response integral $I(\omega_1, \omega_2, t)$ will obviously not vary at this rate, and hence, to increase numerical efficiency, it can be evaluated at a much lower rate. For practical considerations, the cube-root of the dissipation rate values are used, $\varepsilon^{1/3}$.

Recall that the purpose of these in situ measurements is to generate an "automated PIREP" product for use by the aviation and meteorological communities. To this end, a number of practical considerations must be addressed. Due to limited bandwidths and transmission costs, a compromise must be made between the quantity and resolution of the information that is downlinked from aircraft in-flight.

Balancing these practical considerations is the operational utility of the information. Atmospheric turbulence can occur in patches of relative homogeneity, in extremely discrete and localized bursts, or a mixture of the two. A pilot may be more interested in the maximum intensity along the flight path, whereas the important information for the forecaster or numerical weather model may be the average intensity in a given volume of airspace. The techniques that have been detailed in this article, are probably most suited to the "locally-homogeneous" turbulence patches. A number of alternative methods for detecting and quantifying the extreme gust events were examined, including: the classical "derived gust velocity," so-called "level-crossing" methods, statistical extreme value theories, and time-domain aircraft response methods. For a variety of reasons, none of these techniques were adequate for our real-time application.

In order to meet the often contradictory requirements discussed above, the following compromise reporting methods were adopted. The reporting interval was chosen as 1 min, which corresponds to a spatial resolution of approximately 10–15 km for a typical commercial transport in cruise. For each of these intervals, the median and 90th percentile of the "per-data-update" $\varepsilon^{1/3}$ values were computed, corresponding to "average" and "peak" intensities.

Figures 5–8 illustrate the results of our methods. For the research aircraft data, "ground truth" dissipation rate values were calculated via consistent techniques applied to the vertical gust velocities. That is, applying Eqs. (20), (23), and (38)—without the aircraft response function—to get $\varepsilon^{1/3}$ in terms of σ^2_{wg}. For the "lower-quality" transport aircraft data, there was a large uncertainty in the gust velocities, hence, the vertical velocity spectra were used to estimate the "truth" eddy dissipation values.

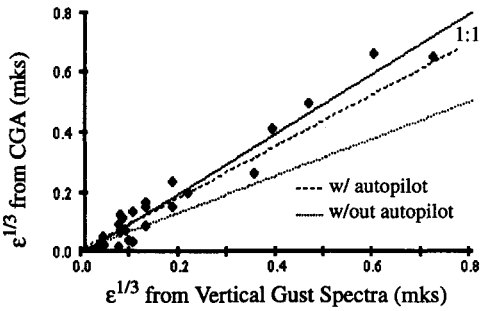

Fig. 7 Same as Fig. 5, using lower quality large transport aircraft data. Correlation coefficient is 0.97.

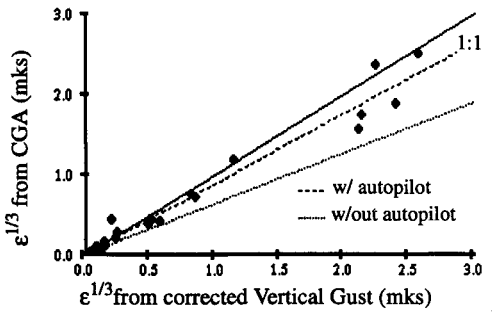

Fig. 8 90th percentile eddy dissipation rate values from large transport aircraft data. Correlation coefficient is 0.98.

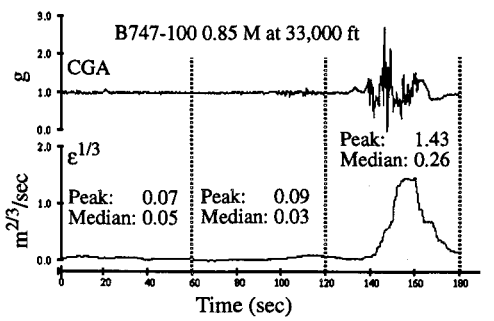

Fig. 9 Detailed time history for severe transport encounter.

Figure 9 shows a detailed time-history from one of the severe large transport encounters. It is clear that reporting both the average and peak $\varepsilon^{1/3}$ values is crucial. Furthermore, it can be seen that while the peak $\varepsilon^{1/3}$ value may not be justified on theoretical grounds, it does detect and indicate the relative severity of this very localized and intense turbulence event.

Conclusions

A new method for computing an atmospheric turbulence intensity metric—the eddy dissipation rate—has been presented. This method, while using standard techniques, is unique in that all simplifying assumptions are explicitly accounted for. Attempts were made to minimize computational complexity while ensuring accuracy and wide applicability. Preliminary results indicate the viability of these techniques and the promise of generating accurate, quantitative, and timely turbulence measurements from commercial transport aircraft.

Acknowledgments

This research is sponsored by the National Science Foundation through an Interagency Agreement in response to requirements and funding by the Federal Aviation Administration's Aviation Weather Development Program. The views expressed are those of the authors and do not necessarily represent the official policy or position of the U.S. Government.

References

[1]Hoblit, F. M., *Gust Loads on Aircraft: Concepts and Application*, AIAA Education Series, AIAA, Washington, DC, 1988.

[2]Houbolt, J. C., Steiner, R., and Pratt, K. G., "Dynamic Response of Airplanes to Atmospheric Turbulence Including Flight Data on Input and Response," NASA TR-199, June 1964.

[3]Panofsky, H. A., and Dutton, J. A., *Atmospheric Turbulence*, Wiley, New York, 1984.

[4]Hinze, J., *Turbulence*, McGraw-Hill, New York, 1975.

[5]Kolmogorov, A. N., "The Local Structure of Turbulence in Incompressible Viscous Fluid for Very Large Reynold's Numbers," *Doklady Akademii Nauk SSSR*, Vol. 30, No. 4, 1941, pp. 299–303.

[6]Von Kármán, T., "Progress in the Statistical Theory of Turbulence," *Journal of Marine Research*, Vol. 7, No. 3, 1948, pp. 252–264.

[7]Gossard, E., and Strauch, R. G., *Radar Observation of Clear Air and Clouds*, Elsevier, Amsterdam, 1983.

[8]Taylor, G. I., "The Spectrum of Turbulence," *Proceedings of the Royal Society, Section A*, Vol. 164, No. 919, 1938, pp. 476–490.

[9]Mark, W. D., and Fischer, R. W., "Investigation of the Effects of Nonhomogeneous (or Nonstationary) Behavior on the Spectra of Atmospheric Turbulence," NASA CR-2745, Oct. 1976.

[10]MacCready, P. B., Jr., "Standardization of Gustiness Values from Aircraft." *Journal of Applied Meteorology*, Vol. 3, No. 13, 1964, pp. 439–449.

[11]Lee, Y., "Preliminary Results of the 1983 Coordinated Aircraft—Doppler Weather Radar Turbulence Experiment," Lincoln Lab., Massachusetts Inst. of Technology, Project Rept. ATC-137, Cambridge, MA, 1988.

[12]Poellot, M. R., and Grainger, C. A., "A Comparison of Several Airborne Measures of Turbulence," Preprints, Fourth International Conference of the Aviation Weather System, Paris, France, American Meteorological Society, Boston, MA, 1991.

[13]Houbolt, J. C., and Williamson, G., "Spectral Gust Response for an Airplane with Vertical Motion and Pitch," Air Force Flight Dynamics Lab., TR-75-121, Wright-Patterson AFB, OH, Oct. 1975.

[14]Goldberg, J. H., "Gust Response of Commercial Jet Aircraft Including Effects of Autopilot Operation," NASA CR-NAS1-16095, June 1982.

[15]Houbolt, J. C., private communication, Williamsburg, VA, 1993.

[16]Lanning, J. H., and Battin, R. H., *Random Processes in Automatic Control*, McGraw-Hill, New York, 1956.

[17]McRuer, D., Ashkenas, I., and Graham, D., *Aircraft Dynamics and Automatic Control*, Princeton Univ. Press, Princeton, NJ, 1973.

[18]Wingrove, R. C., Bach, R. E., and Schultz, T. A., "Analysis of Severe Atmospheric Disturbances from Airline Flight Records," AGARD Flight Mechanics Panel Symposium, Norway, May 1989.